Numerical simulation of the interaction between solar granules and small-scale magnetic fields

I. N. Atroshchenko and V. A. Sheminova

Main Astronomical Observatory, National Academy of Sciences of the Ukraine,
27 Akademika Zabolotnogo St., 03680 Kyiv, Ukraine

Abstract

We have carried out numerical simulation based on the equations of radiation magnetohydrodynamics to study the interaction of solar granules and small-scale magnetic fields in photospheric regions with various magnetic fluxes. Four sequences of 2D time-dependent models were calculated for photospheric regions with average vertical magnetic fluxes of 0, 10, 20, and 30 mT. The models exhibit no substantial variations in their temperature structure with varying average field strength, while the density and gas pressure profiles display gross changes. The solar granulation brightness field also varies substantially with magnetic flux. The contribution of the small-scale component to the intensity power spectrum increases with average field strength, whereas the large-scale component (of about a granule size) contributes less, the total rms intensity fluctuations being approximately the same. Thus the observed decrease in rms intensity fluctuations with growing average magnetic flux can be interpreted as smoothing of the small-scale component in the power spectrum by the modulation transfer function of the telescope.

1 Introduction

The interaction of solar granules and small-scale magnetic elements is of obvious interest, since about 90 percent of the total magnetic flux emerging from the solar photosphere is localized in these elements [21]. On the one hand, formation of small-scale elements is conditioned by the granulation scale of solar convection. On the other hand, the small-scale magnetic fields can have a profound impact on the solar granulation dynamics and structure. Thus theoretical models of small-scale concentrations should incorporate this scale of solar convection. Magnetic tubes are observed in the continuum as a network of bright points located in intergranular lanes [14]. The size of these points is beyond the resolution possibility of today's telescopes, so that the fine structure of these small-scale concentrations need be studied by combining theoretical methods [18, 19] with various observational data such as Stokes profiles of spectral lines [20], line asymmetries [3, 9], observations with high spatial resolution [23].

By now a large number of semiempirical models of magnetic tubes have been developed, they are able to account, at least qualitatively, for the structure of small-scale magnetic elements and to reproduce the observed Stokes profiles of solar spectral lines in magnetic regions. However, totally self-consistent models of small-scale magnetic elements

can be constructed only on the basis of the equations of radiation magnetohydrodynamics. Three-dimensional simulation of solar magnetoconvection was done by Nordlund [15] and Nordlund and Stein [6, 17], but the spatial resolution of their models is too small (the horizontal step of calculation grid is 100–200 km) to reproduce magnetic tubes of about 100 km in size. Deinzer et al. [4,5], Knölker et al. [11], Grossman-Doerth et al. [7] calculated detailed 2D models of small-scale magnetic tubes with a high spatial resolution. These models throw light on the dynamics and fine structure of small-scale magnetic concentrations [18], but they deal with single tubes only and ignore the interaction of tubes with each other.

Here the object is to study the interaction between solar granulation and small-scale magnetic fields in photospheric regions with different magnetic fluxes. A detailed 3D simulation of this interaction requires an excessively great number of points in the calculation mesh and hence a prohibitively long machine time, so we used a complete set of 2D equations of radiation magnetohydrodynamics in the Cartesian coordinates for the solution of this problem. The basic idea was to construct solar granulation models with magnetic fields neglected and then to calculate a sequence of models with different densities of average magnetic flux with the same boundary and initial conditions (except for the initial magnetic field). In this way we could follow the influence of magnetic fields on granulation properties, brightness field, and fine structure of intergranular lanes, where magnetic tubes are formed. We note that we deal with magnetic fluxes on a plane (magnetic slabs) in the 2D simulation, while these objects are magnetic flux tubes in actuality, they are simply called magnetic tubes. To avoid confusion, we use the term magnetic tubes in what follows.

2 Radiation magnetohydrodynamics equations

To simulate the interaction between solar granulation and small-scale magnetic fields, we used the complete set of 2D equations of radiation magnetohydrodynamics for stratified media in the Cartesian coordinates:

$$\frac{\partial \rho}{\partial t} + \frac{\partial \rho v_j}{\partial x_j} = 0, \tag{1}$$

$$\frac{\partial \rho v_i}{\partial t} + \frac{\partial \rho v_i v_j}{\partial x_j} = -\frac{\partial}{\partial x_i}\left(p + \frac{B^2}{8\pi}\right) + \frac{1}{4\pi}\frac{\partial B_i B_j}{\partial x_j} + \rho g \delta_{i2}, \tag{2}$$

$$\frac{\partial E}{\partial t} + \frac{\partial \rho \epsilon v_j}{\partial x_j} = -\frac{\partial}{\partial x_j}\left[\left(p + \frac{B^2}{8\pi}\right) v_j\right] + \frac{1}{4\pi}\frac{\partial}{\partial x_i}(v_i B_i B_j) - Q_R + Q_j + \rho g v_i \delta_{i2}, \tag{3}$$

$$\frac{\partial B_i}{\partial t} + \frac{\partial}{\partial x_j}(v_j B_i - v_i B_j) = \frac{\partial}{\partial x_j}\eta\left(\frac{\partial B_i}{\partial x_j} - \frac{\partial B_j}{\partial x_i}\right), \tag{4}$$

where i, j vary from 1 to 2, ρ and p are the medium density and gas pressure, v_i are the velocity vector components, B_i are the components of the magnetic flux density vector, g is the vertical component of the gravitation vector, δ_{i2} is the Kronecker delta, $\epsilon = e + v_i^2/2$

is the sum of the internal and kinetic energy per unit mass, $E = \rho\epsilon + B^2/8\pi$ is the total energy per unit volume, Q_R is the divergence of radiant energy flux. The magnetic diffusion coefficient is a function of temperature, $\eta = \eta(T)$. The term Q_j specifies the Joule dissipation:

$$Q_j = \frac{\eta}{4\pi}\left(\frac{\partial B_i}{\partial x_j} - \frac{\partial B_j}{\partial x_i}\right)^2. \tag{5}$$

The gas pressure was found from the equation of state for a partially ionized gas:

$$p = p(\rho, e). \tag{6}$$

The equation of state was calculated beforehand, and then, during calculations, the pressure p was found from tables.

Turbulence effects were assumed to be simulated by numerical viscosity.

3 Radiative transfer

The quantity Q_R, which specifies the radiative interaction between matter and radiation field in Eq. (3), was calculated from the relation

$$Q_R = 4\pi \int_0^\infty \alpha_\nu (B_\nu - J_\nu) d\nu, \tag{7}$$

where J_ν is the mean intensity, α_ν and B_ν are the absorption coefficient and the Planck function for the frequency ν. To find Q_R, we solved the radiative transfer equation for each time step:

$$\frac{\partial}{\partial x}\frac{1}{\alpha_\nu}\frac{\partial}{\partial x}(f_{\nu xx} J_\nu) + \frac{\partial}{\partial z}\frac{1}{\alpha_\nu}\frac{\partial}{\partial z}(f_{\nu zz} J_\nu) = \alpha_\nu (J_\nu - B_\nu), \tag{8}$$

where $f_{\nu xx}$ and $f_{\nu zz}$ are the Eddington factors. The factors $f_{\nu zz}$ were determined from the 1-D solution of the radiative transfer equation along the OZ direction, while the factors $f_{\nu xx}$ were assumed to be 1/3 (this procedure is described in detail in [1]). Lateral boundary conditions were assumed to be periodic, and this suggested that the matter penetrated freely through the lateral boundary on one side and flew out with the same parameters on the opposite side. The upper and lower boundary conditions for Eq. (8) were taken in accordance with Mihalas [13]. At the lower boundary, where the diffusion approximation is valid, we have

$$\frac{\partial f_{\nu zz} J_\nu}{\partial z} = \frac{1}{3}\frac{\partial B_\nu}{\partial z}, \tag{9}$$

and at the upper boundary we have

$$\frac{\partial f_{\nu zz} J_\nu}{\partial z} = \alpha_\nu h_\nu J_\nu. \tag{10}$$

Here $h_\nu = H^0_\nu / J_\nu$, H^0_ν being the vertical radiation flux at the upper boundary. The factor h_ν was found from the 1-D solution of the radiative transfer equation in the OZ direction. Equation (8) was solved by the iteration method. For the simulation of upper photospheric layers to be correct, we allowed for the radiative transfer in spectral lines, as the energy is reradiated in this region predominantly in line frequencies. This was done with the OPDF table by Kurucz [12]. The whole frequency range was divided into four frequency groups depending on the total absorption coefficient (continuum + line opacities). The Planck function and the Rosseland mean absorption coefficient were tabulated for each frequency group. Thus radiative transfer equation (8) was first solved for four opacity groups and for each trime step, and then the integral quantity Q_R was found with relation (7), each frequency range being taken with its weight.

4 Calculation procedure

To integrate the complete set of MHD equations (1)–(4), we used the conservative Total Variation Diminishing (TVD) scheme [8]. The principal concept of the scheme is to set limits on the general variation of numerical solution and prevent formation of nonphysical oscillations. The TVD scheme is second-order accurate in regions with a smooth solution, and it switches over to the first-order "against-the-flux" scheme near extrema.

For the simple transfer equation

$$\frac{\partial u}{\partial t} + \frac{\partial f}{\partial x} = 0, \tag{11}$$

where

$$f = \alpha u, \tag{12}$$

the TVD scheme can be written as in [6]:

$$u^{n+1} = u^n - \frac{\Delta t}{\Delta x}(F^n_{i+1/2} - F^n_{i-1/2}), \tag{13}$$

where $F_{i+1/2}$ is the numerical flux

$$F_{i+1/2} = 0.5(f_{i+1} + f_i) - 0.5|a_{i+1/2}|[1 - \phi(r_{i+1/2})](u_{i+1} - u_i), \tag{14}$$

$\phi(r_{i+1/2})$ is a switching function which depends on the ratio between the numerical gradients calculated in accordance with the flux direction:

$$r_{i+1/2} = \frac{u_{i+1-\sigma} - u_{i-\sigma}}{u_{i+1} - u_i}, \tag{15}$$

with $\sigma = sign(\alpha_{i+1/2})$. The switching function in this study was

$$\phi(r) = \begin{cases} 2, & when \quad r > 2, \\ r, & when \quad 0 < r \leq 2, \\ 0, & when \quad r \leq 0. \end{cases}$$

It switched TVD scheme (13)–(14) to a second-order scheme in regions with a smooth solution, $\phi(1) = 1$, and to the first-order "against-the-flux" scheme near extrema, where $\phi(r < 1) = 0$.

The second-order Adams–Bashforth scheme was used for the sampling of Eqs (1)–(4).

5 Boundary and initial conditions

We assumed the lateral boundary conditions to be periodic. The boundary conditions at the upper boundary were taken open, but vertical velocities were scaled so that the mass flow through the upper boundary might be zero. Mean density and mean internal energy were specified by initial conditions, and their fluctuations were scaled so that the solution near the boundary might be smooth. A firm wall with a fixed internal energy was postulated at the bottom of the box simulated. We assumed that

$$\frac{\partial B_x}{\partial z} = 0 \tag{16}$$

for the magnetic field at the upper and the lower boundaries.

The initial distribution of thermodynamic quantities was taken uniform at all horizontal levels, it was specified by the VAL80C model [24] for upper layers and by a model envelope calculated on the basis of the mixing-length theory [2] for deeper layers. A solenoidal velocity field in the form of a sum of harmonic functions,

$$u(x,z) = \sum_{l=1}^{128} A_l \sin(k_{xl}x) \exp[-k_{zl}(z_{max} - z)], \tag{17}$$

$$w(x,z) = \sum_{l=1}^{128} A_l \cos(k_{xl}x) \exp[-k_{zl}(z_{max} - z)], \tag{18}$$

was introduced in the model to initiate convection in order to provide the greatest number of granulation motion scales in the box.

The simulated region was represented by 256×128 cells of calculation mesh with the step $\Delta x = \Delta z = 15$ km, it was rectangular in shape, 3840 km wide and 1920 km high. The upper boundary corresponded to the height $h = 600$ km above the $\tau_R = 1$ level.

The above algorithm was used to calculate a sequence of nonmagnetic models (with no magnetic field) for a simulation time of 16 min (which corresponds approximately to three passages of acoustic waves in the region). The matter in the box makes several revolutions in this time, and a statistically stable solution sets in. Then we introduced a vertical uniform magnetic field with different intensities into the model. Thus a nonmagnetic model was employed as an initial condition for simulating magnetoconvection. The primary idea of the numerical experiment was to study changes in the solar granulation structure and properties in photospheric regions with different mean magnetic fluxes. With boundary and initial conditions specified, we have a single free parameter in the problem – the initial magnetic field intensity. In this numerical experiment we calculated four model sequences in the time interval from 16 to 25 min with initial mean magnetic field intensities of 0, 10, 20, 30 mT.

6 The solar granulation dynamics and structure depending on magnetic flux

Figure 1 shows the vertical and horizontal rms velocities in relation to the horizontally-averaged Rosseland optical depth for models with different magnetic fluxes. Our 2D

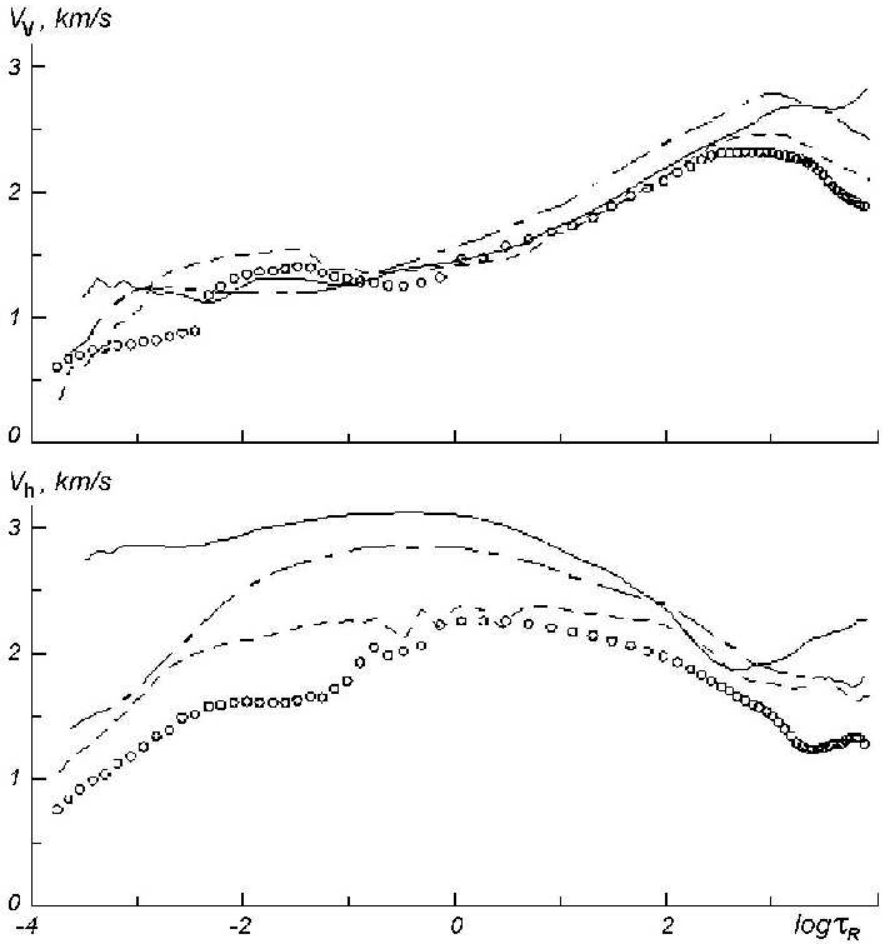

Figure 1: Vertical and horizontal rms velocities (V_v and V_h) as functions of the horizontally-averaged Rosseland optical depth for models with different mean magnetic fluxes: solid line) 0 mT, dot-and-dash line) 10 mT, dashed line) 20 mT, circles) 30 mT.

models being nonstationary, the velocities in Fig. 1 are averaged for each sequence of five models over 20–25 min intervals. As the initial magnetic field in our models is vertically directional, the mean field intensity has no pronounced effect on vertical velocities, while horizontal velocities are appreciably suppressed by the magnetic field in the upper layers, where the magnetic pressure exceeds or is comparable to the gas pressure.

The simulation results do not reveal any substantial changes in the averaged structure of the models depending on magnetic flux, but the fluctuation profiles of thermodynamic quantities vary considerably with magnetic flux. Fluctuations in the total pressure in the upper layers diminish with growing magnetic flux due to the suppression of horizontal motions by the vertical magnetic field, i.e., the models tend to a quasi-equilibrium state in the horizontal direction with growing magnetic flux. At the same time relative fluctuations in the gas pressure and density increase with magnetic flux density owing to the growing magnetic pressure fluctuations.

Figure 2a depicts the structure of the velocity field and temperature field for the models with a simulation time of 25 min and different mean magnetic fluxes. Temperature inhomogeneities of about granule size become more smoothed with increasing mean field intensity, while the fluctuations in intergranular lanes grow. Temperature fluctuations in the optically thin upper layers are governed primarily by radiative transfer, that is why

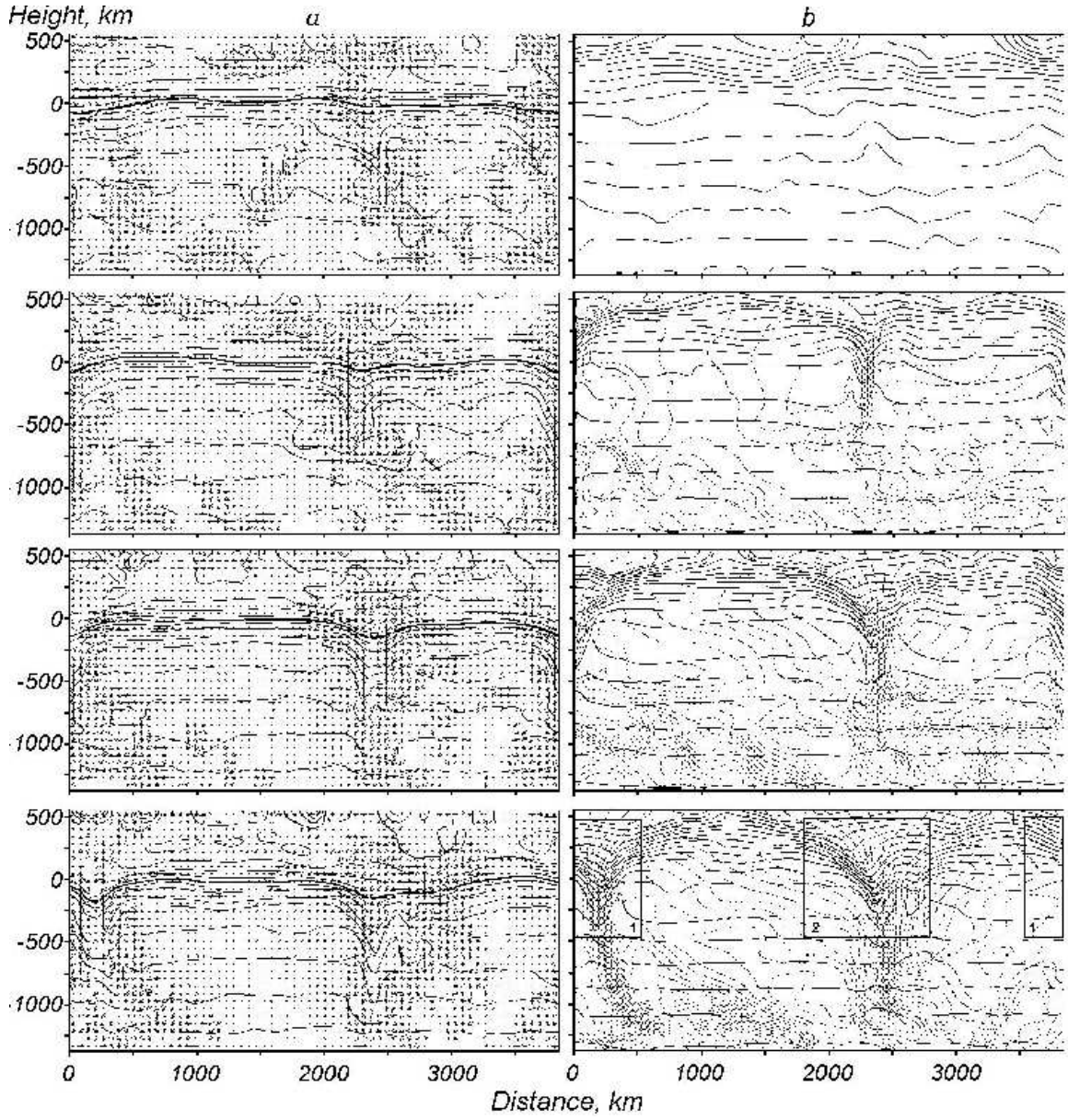

Figure 2: Results of simulation: a) isotherms (lines) and velocity field (arrows); thick line shows a 6400 K isotherm, which corresponds approximately to the level $\tau_R = 1$ for homogeneous models; b) isopycnics (thick lines) and lines of magnetic field force (thin lines). The simulation time is 25 min. Mean vertical magnetic field intensity is 0, 10, 20, and 30 mT (from top to bottom).

the temperature fluctuations at small optical depths are close in magnitude in all models. The area occupied by downflows increases as well, and regions where the velocities are suppressed by magnetic fields appear in intergranular lanes in the models with a mean magnetic flux of 20 mT or higher.

Figure 2b shows isopycnics together with lines of magnetic force. The solar convection is known to gather the lines of magnetic force together and form vertical bundles in intergranular lanes. The vertical structure of magnetic tubes is lost near the base of the region simulated, since the convective cells are closed in this region because of closed boundary conditions, and the velocities become predominantly horizontal, thus leading to the destruction of vertical structure of magnetic tubes. The magnetic tubes expand in the upper photosphere due to decreasing pressure with growing height, they become thicker, and the area occupied by them grows with the mean field intensity. While the model temperature structure is not markedly affected by variations in the mean magnetic flux, the pressure distribution changes drastically. Abrupt density drops appear in intergranular lanes, the widths of these drops grows with the width of magnetic tubes, and magnetic tubes occupy a considerable part of the area in models with a mean intensity of 30 mT. Density profiles above granules become more sinuous.

7 Fine structure of magnetic tubes

Figure 3 illustrates the structure of a magnetic tube on an enlarged scale. Isopycnics and lines of magnetic force are drawn together with the velocity field for geometric area 2 shown by a square in Fig. 2b. Drops in density profiles grow with magnetic flux. Motions in intergranular lanes are suppressed by the magnetic field. Downward streams flow around the magnetic tube, and so the area occupied by them increases. An interesting effect can be seen in the area with a 30 mT mean intensity. The magnetic tube becomes thicker and breaks up into two tubes. Motions are found to be suppressed in the space between two tubes, while there are downflows inside the tubes. This is likely to be a structure intermediate between a facular point and a pore; a similar configuration was simulated by Knölker et al. [10]. Unlike in the magnetic tube in region 2, motions in the tube lying in geometric region 1 (Fig. 2b) are completely suppressed by the magnetic field at a mean intensity greater than 10 mT. This tube resembles the classical magnetic tube model.

The surface of equal gas and total (gas + magnetic) pressures for the geometric regions shown by squares 1 and 2 in Fig. 2b is a tube-like structure of small-scale magnetic elements. The width of drops in the gas pressure profile grows with magnetic field intensity. Two drops in the gas pressure profile can be seen in the models with a mean intensity of 30 mT, where a tube breaks up into two magnetic tubes (Fig. 3d), but the surface of equal total pressure does not vary with magnetic flux. The total pressure remains approximately constant at all horizontal levels, i.e., the models tend to a quasi-equilibrium state in the horizontal direction while the mean magnetic flux increases.

8 Brightness variations depending on magnetic flux

Continuum intensity profiles calculated for models with different magnetic fluxes for $\lambda = 500$ nm and for a simulation time of 25 min are plotted in Fig. 4. The model with no magnetic field displays bright granules 1000–2000 km in size. The granule brightness amplitude decreases in the models with a magnetic field, but brightness peaks with

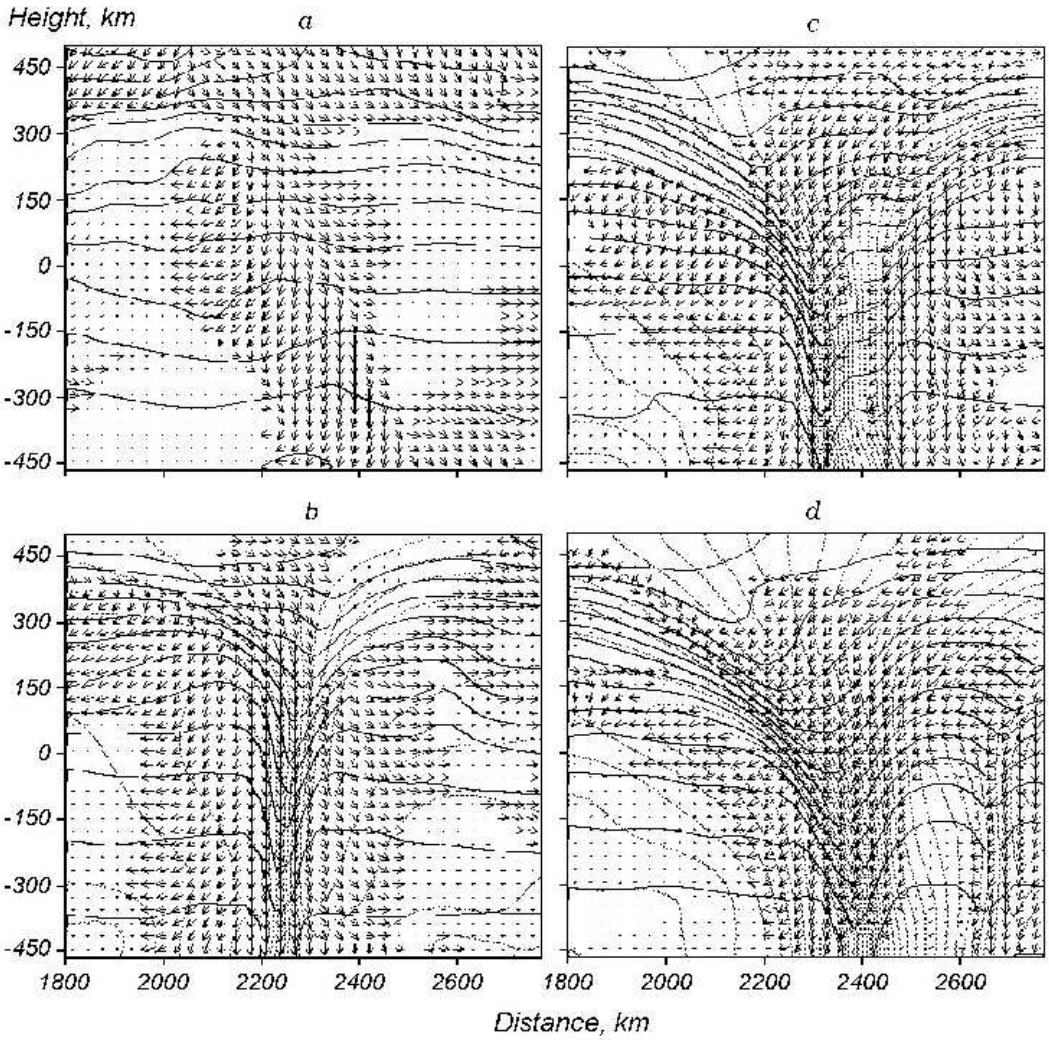

Figure 3: Isopycnics (thick lines), lines of magnetic field force (thin lines), and velocity field for the geometric region shown by square 2 in Fig. 2b on an enlarged scale. Mean vertical magnetic field intensity is 0(a), 10(b), 20(c), and 30(d) mT.

intensities up to 1.6 appear in intergranular lanes. Deinzer et al. [5] point out that these intensity peaks are surrounded by dark rings formed by local peaks in the density profiles near magnetic tube boundaries (Fig. 3). The area occupied by bright points increases with magnetic flux, and the amplitude of large-scale inhomogeneities (about a granule size) decreases. Overall fluctuations of the intensity averaged over five models change only slightly with varying magnetic field intensity, they are about 14% for $\lambda = 500$ nm.

To demonstrate the intensity field "smearing" due to a limited spatial resolution, we convoluted the intensity profiles calculated with 2D models with a modulation transfer function (MTF) for an ideal telescope of diameter $D = 30$ cm. This function was represented by a Gaussian profile with the half-width λ/D. Figure 4 shows the intensity profiles smoothed in this manner. The intensity contrast decreases considerably, and bright points are hardly discernible among granules. Besides, the horizontal dimension of smoothed bright peaks in models with a large mean magnetic flux becomes comparable to the size of small granules. Therefore, it is difficult to distinguish the bright points associated with small-scale magnetic structures from granules in facular plages with large

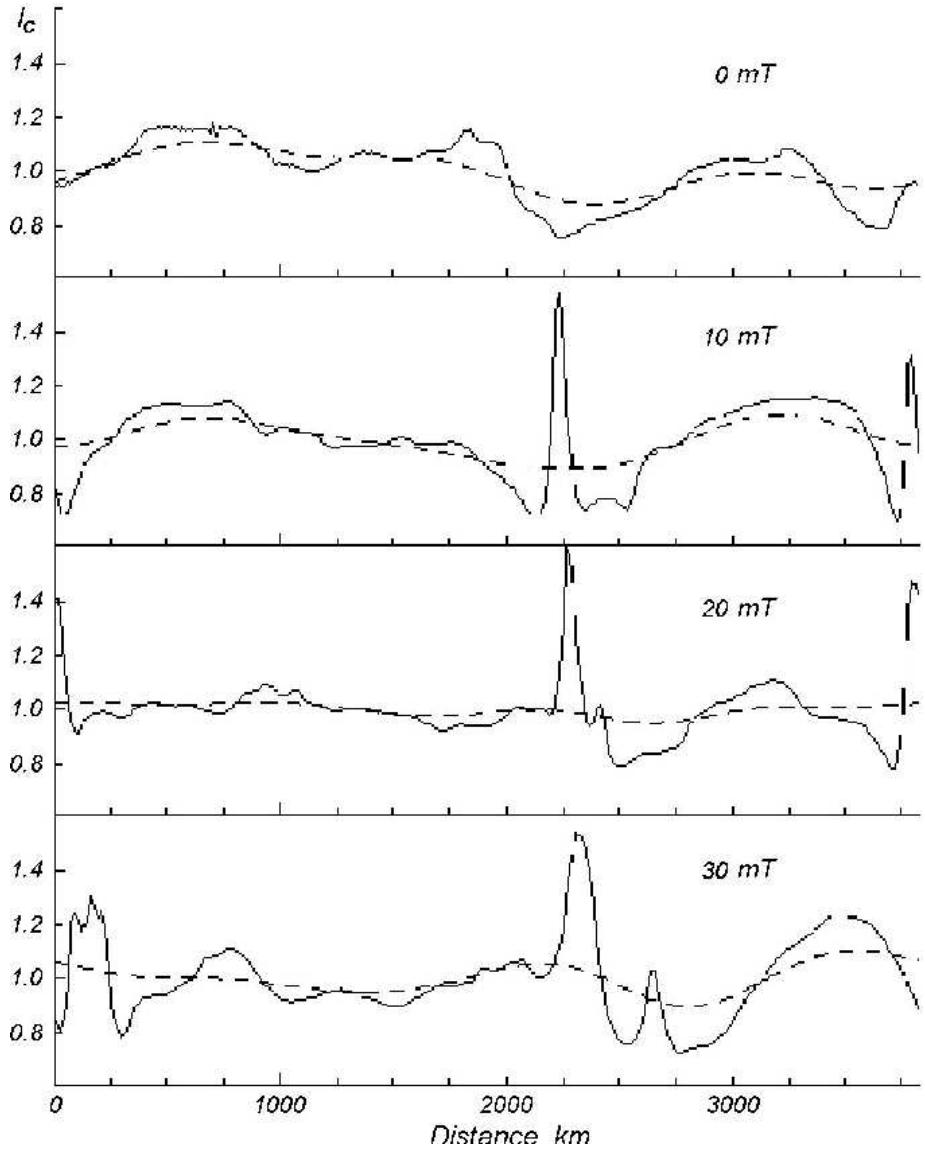

Figure 4: Radiation intensity in the continuum for models with a 25-min simulation time and different mean magnetic fluxes (solid line). Dashed line shows intensity profiles obtained after the convolution with the modulation transfer function of the telescope.

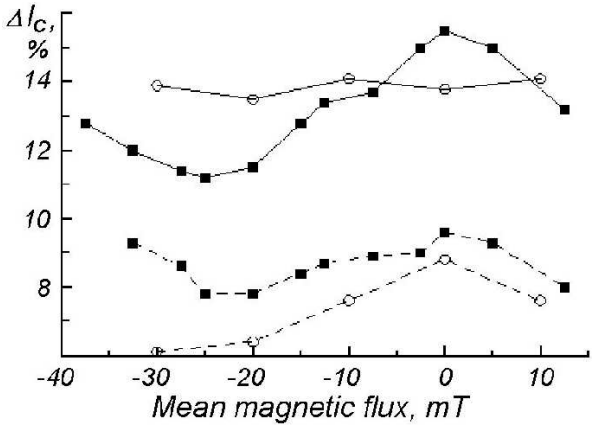

Figure 5: Root-mean-square fluctuations in the continuum intensity calculated for 2-D models (solid line with circles) and smoothed by the modulation transfer function of the telescope (dashed line with circles); original observations (solid line with squares) and observations with 5-min oscillations filtered off (dashed line with squares) from the data of [22].

magnetic filling factors.

The intensity power spectrum averaged over five models with different magnetic fluxes suggests that the small-scale component grows with field intensity while the large-scale component becomes weaker. When observed with a limited spatial resolution, small-scale bright points are smoothed by the telescope MTF, and the observed overall fluctuations of intensity diminish with growing mean magnetic flux.

Figure 5 shows the intensity fluctuations calculated from 2D models and observed with the SOUP space telescope with a 30 cm aperture [22]. As there is no fundamental difference between the positive and negative orientations of the initial magnetic field in our models, the intensity fluctuations were assumed to be symmetric about the zero magnetic field. Obviously the intensity fluctuations calculated from 2D models are approximately at the same level for the field intensity range from 0 to 30 mT, but the fluctuations smoothed by the telescope MTF diminish with growing mean field intensity. The observations in [22] display the same tendency. Thus, the observed decrease of intensity fluctuations in the continuum with increasing mean magnetic flux can be accounted for, at least qualitatively, within the framework of our 2D models.

9 The Wilson depression

The Wilson depression (Fig. 6) is about 150–200 km in the regions of magnetic flux concentration. Bright peaks arise in the continuum, as the horizontal temperature structure varies more smoothly than the height of the layer where the optical depth is unity. Besides, such depressions of the level $\tau_R = 1$ are outlets for the radiant energy from hot lower layers, which results in additional heating of the upper parts of magnetic tubes [11]. The relationship between magnetic flux density and distance (Fig. 6) suggests that there is a clear correlation between magnetic flux in tubes and bright intensity peaks. There is also a clear distinction between small-scale magnetic elements and nonmagnetic regions with a nearly zero magnetic field intensity. The width of magnetic tubes grows with field intensity, but the maximum magnetic flux density in small-scale magnetic structures remains nearly constant and is about 200 mT.

So, we constructed four sequences of model solar photospheres with different magnetic fluxes. When a magnetic field is introduced in the models, three main free parameters appear: initial magnetic field configuration, magnetic diffusion, and initial field intensity. The initial magnetic field orientation, which determines the predominant direction of magnetic flux, was fixed in our simulation (the initial magnetic field was assumed to be vertical). The magnetic diffusion coefficient specifies the maximum concentration of magnetic flux density and, consequently, other parameters that depend on these quantities such as drops in pressure and density, the Wilson depression in the magnetic tube. The magnetic diffusion coefficient was a function of temperature in the simulation and was defined by one and the same law for all models. In the calculations we chose the smallest magnetic diffusion coefficient that ensured a stable numerical solution, it was about $\eta = 10^{16}$ cm^{2}s^{-1} at $T = 10000$ K. Thus, only the initial field intensity was varied in our models. The maximum magnetic flux density being limited by the magnetic diffusion coefficient, a growth of the mean magnetic flux resulted in widening of magnetic tube, i.e., in an increase of magnetic filling factor. The filling factor for MHD models should be estimated, however, from 3D calculations, since the topologies of 2D and 3D convective motions are fundamentally different.

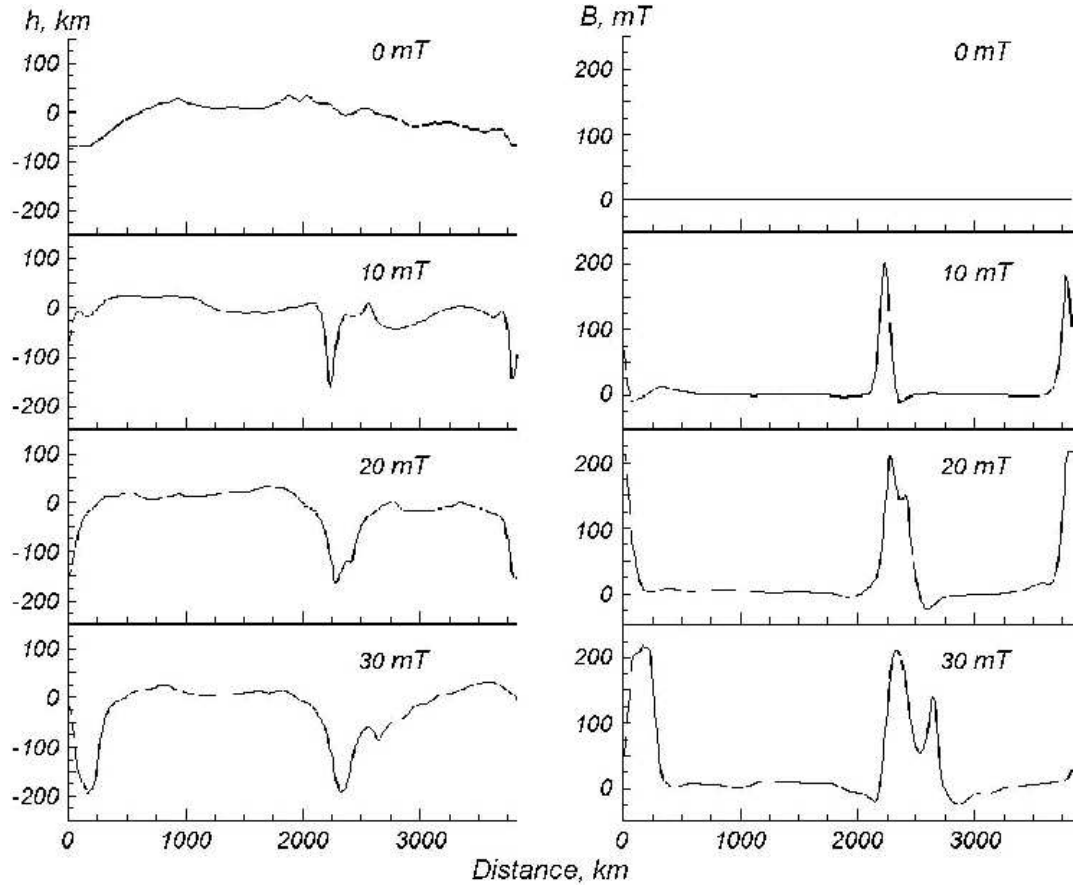

Figure 6: Geometric height for the optical depth $\tau_R = 1$ (a) and vertical magnetic flux density at the level $\tau_R = 1$ (b) v. horizontal distance for models with different mean magnetic fluxes.

10 Conclusion

The major results of our study are as follows.

1. A vertical magnetic field with a mean intensity of 10–30 mT has no appreciable effect on vertical velocities, while horizontal velocities are suppressed to a considerable degree by the field.

2. Fluctuations in the total pressure diminish with growing mean field intensity owing to the suppression of horizontal velocities by a vertical magnetic field, i.e., the models tend to a quasi-equilibrium state in the horizontal direction when the magnetic flux increases.

3. Fluctuations in the relative gas pressure and density grow with field intensity, while the temperature fluctuations grow in subphotospheric layers only and become approximately the same in all models at the upper levels.

4. Gas motions are suppressed inside magnetic tubes in the models with a mean intensity of 20 mT and higher.

5. A peculiar configuration appears in the models with a mean field intensity of 30 mT: a thick tube breaks up into two tubes, with motions suppressed in the region between the tubes rather than inside the tubes. This is likely to be a structure intermediate between a facular point and a pore.

6. A magnetic field affects only slightly the overall fluctuations of the continuum intensity, but changes substantially the intensity power spectrum. The contribution of the

small-scale component to the intensity power spectrum grows with magnetic flux, while the contribution from the large-scale component (of about a granule size) diminishes, so that observations with a limited spatial resolution show a decrease of intensity fluctuations with growing magnetic flux, as small-scale bright spots are smoothed by the modulation transfer function of the telescope.

The approach elaborated here has some limitations and disadvantages. The two-dimensional representation of granulation motions is the crudest assumption in our treatment. Magnetic tubes in our models are formed between two granules, while small-scale elements in the solar photosphere are observed in the lanes formed by at least three or more neighboring granules. We dealt with the granular scale of solar convection only, and the initial magnetic field was artificially introduced in the models. Formation of initial field need be studied before the formation of facular plages and network areas can be understood. This problem can be studied by simulating larger solar convection scales such as meso- and supergranulation.

In spite of the shortcomings of our method, the 2D models calculated by us can be used for the interpretation of observational data for solar photospheric regions with various mean magnetic fluxes. The models will be applied in our subsequent studies to calculate profiles of actual solar photospheric lines.

Acknowledgments. We wish to thank A. S. Gadun for useful discussion of the results.

References

[1] I. N. Atroshchenko, "Three-dimensional hydrodynamic models of the solar photosphere," Kinematika i Fizika Nebesn. Tel [Kinematics and Physics of Celestial Bodies], vol. 9. no. 1, pp. 3–15, 1993.

[2] I. N. Atroshchenko and A. S. Gadun, "Approximate models of the solar convection zone in a modified mixing length theory approximation," ibid., vol. 2, no. 4, pp. 21–26, 1986.

[3] P. N. Brandt and A. S. Gadun, "Changes in the parameters of FeI spectral lines as a function of the magnetic flux (solar disk center)," ibid., vol. 9, no. 3, pp. 8–22, 1993.

[4] W. Deinzer, G. Hensler, M. Schüssler, and E. Weisshaar, "Model calculations of magnetic flux tubes. I. Equations and method," Astron. and Astrophys., vol. 139, no. 2, pp. 426–434, 1984.

[5] W. Deinzer, G. Hensler, M. Schüssler, and E. Weisshaar, "Model calculations of magnetic flux tubes. II. Stationary results for solar magnetic elements," ibid., vol. 139, no. 2, pp. 435–449, 1984.

[6] C. A. J. Fletcher, Computational Techniques for Fluid Dynamics, Vol. 2, Springer, Berlin, 1988.

[7] U. Grossmann-Doerth, M. Knölker, M. Schüssler, and E. Weisshaar, "Models of magnetic flux sheets," in: Solar and Stellar Granulation, R. J. Rutten and G. Severino (Editors), pp. 481–490, Kluwer, Dordrecht, 1989.

[8] A. Harten, J. Comput. Phys., vol. 49, p. 357, 1983.

[9] S. I. Kiel, Th. Rondier, E. Cambell, et al., "Observation and interpretation of photospheric line asymmetry changes near active regions," in: Solar and Stellar Granulation, R. J. Rutten and G. Severino (Editors), pp. 273–286, Kluwer, Dordrecht, 1989.

[10] M. Knölker and M. Schüssler, "Model calculations of magnetic flux tubes. IV. Convective energy transport and the nature of intermediate size concentrations," Astron. and Astrophys., vol. 202, no. 1/2, pp. 275–283, 1988.

[11] M. Knölker, M. Schüssler, and E. Weisshaar, "Model calculations of magnetic flux tubes. III. Properties of solar magnetic elements," ibid., vol. 194, no. 1/2, pp. 257–267, 1988.

[12] R. I. Kurucz, "Model atmospheres for G, F, A, and O stars," Astrophys. J. Suppl. Ser., vol. 40, pp. 1–340, 1979.

[13] D. Mihalas, Stellar Atmospheres, Freeman, San Francisco, 1978.

[14] R. Müller, "Fine structure of photospheric faculae," in: Solar Photosphere: Structure, Convection and Magnetic Fields, R. J. Rutten and G. Severino (Editors), pp. 85–96, Kluwer, Dordrecht, 1990.

[15] Å. Nordlund, "The 3D structure of the magnetic field and its interaction with granulation," in: Theoretical Problems in High-Resolution Solar Physics, H. U. Schmidt (Editor), pp. 101–119, Munchen, 1985.

[16] Å. Nordlund and R. F. Stein, "Simulating magnetoconvection," in: Solar and Stellar Granulation, R. J. Rutten and G. Severino (Editors), pp. 453–468, Kluwer, Dordrecht, 1989.

[17] Å. Nordlund and R. F. Stein, "Solar magnetoconvection," in: Solar Photosphere: Structure, Convection and Magnetic Fields, R. J. Rutten and G. Severino (Editors), pp. 191–211, Kluwer, Dordrecht, 1990.

[18] M. Schüssler, "Theoretical aspects of small-scale photospheric magnetic fields," in: Solar Photosphere: Structure, Convection and Magnetic Fields, R. J. Rutten and G. Severino (Editors), pp. 161–179, Kluwer, Dordrecht, 1990.

[19] S. K. Solanki, "Small-scale physics of convection and magnetic fields," in: Solar Physics and Astrophysics at Interferometric Resolution, L. Dame and T.-D. Guyenne (Editors), pp. 27–33, ESA Spec. Publ., 1992.

[20] S. K. Solanki, "Small-scale solar magnetic fields: an overview," Space Sci. Rev., vol. 63, pp. 1–¡-¿88, 1993.

[21] J. O. Stenflo, "Small-scale magnetic structure of the Sun," Astron. and Astrophys. Rev., vol. 1, pp. 3–46, 1989.

[22] A. M. Title, T. D. Tarbell, K. P. Topka, et al., "Flows, random motions and oscillation in solar granulation derived from the SOUP instrument on SPACELAB 2," in: Solar and Stellar Granulation, R. J. Rutten and G. Severino (Editors), pp. 225–251, Kluwer, Dordrecht, 1989.

[23] A. M. Title, R. A. Shine, T. D. Tarbell, et al., "High-resolution observations of the photosphere," in: Solar Photosphere: Structure, Convection and Magnetic Fields, R. J. Rutten, and G. Severino (Editors), pp. 49–66, 1990.

[24] J. E. Vernazza, E. H. Avrett, and R. Loeser, Structure of the Solar Chromoshere. III. Models of the EUV Brightness Components of Quiet Sun, Preprint No. 1308, Center for Astrophysics, Cambridge, 1980.